ChemComm

COMMUNICATION

View Article Online
View Journal | View Issue

Cite this: *Chem. Commun.*, 2015, **51**, 7023

Received 7th March 2015,
Accepted 16th March 2015

DOI: 10.1039/c5cc01935d

www.rsc.org/chemcomm

Enhanced photoelectrochemical aptasensing platform based on exciton energy transfer between CdSeTe alloyed quantum dots and SiO_2@Au nanocomposites†

Gao-Chao Fan,[a] Hua Zhu,[a] Qingming Shen,[b] Li Han,[ab] Ming Zhao,[a] Jian-Rong Zhang*[ac] and Jun-Jie Zhu*[a]

High-efficient exciton energy transfer between CdSeTe alloyed quantum dots and SiO_2@Au nanocomposites was applied to develop an enhanced photoelectrochemical aptasensing platform with ultrahigh sensitivity, good selectivity, reproducibility and stability.

The photoelectrochemical technique is a newly emerged yet vibrantly developing analytical method for biological assays. Inherited from the electrochemical method, photoelectrochemical detection has the obvious merits of simple devices, low cost and easy miniaturization compared to optical methods.[1] Moreover, thanks to the different energy forms of the excitation source and detection signal, it is quite sensitive due to the reduced background signals.[2] Accordingly, the photoelectrochemical technique has attracted especial research interest, and various target analytes such as biomarkers, DNA sequences, cancer cells, and small molecules have been successfully determined by this method.[3] Although different types of photoelectrochemical assays have been developed, the detection principle is the same; a photocurrent change can be produced by biological interactions between the biosensing elements and their corresponding target analytes. So far, several strategies have been applied to produce the photocurrent change when biorecognition events occur, such as steric-hindrance effects,[4–6] enzymatic reactions,[7–9] sensitization effects,[10–12] and energy transfer.[13–15] Among them, energy transfer is a promising and powerful tool for the sensitive detection of various biomolecules by changing the distance between energy donors and acceptors.

Photoelectrochemical energy transfer is inspired by luminescence resonance energy transfer (LRET), which is a nonradiative process wherein photoactive donors transfer exciton energy to proximal acceptors *via* nonradiative dipole–dipole interactions.[16] Of course, the generation of energy transfer is closely dependent on the absorption and emission spectral overlap as well as the distance between the energy donor and acceptor (10 ± 2 nm). Recently, semiconductor quantum dots (QDs) have proved to be the best candidates for photoelectrochemical energy donors because of their prominent features of photochemical stability, broad excitation, tunability of emission spectra, and binding compatibility with biomolecules.[17] Metallic nanoparticles (NPs), especially Au NPs, were widely used as photoelectrochemical energy acceptors due to their strong surface plasmon resonance (SPR), as well as high extinction coefficient and broad absorption spectra.[13] For energy transfer based photoelectrochemical biosensing, nearly all of the work only emphasized the spectral overlap and the distance between the semiconductor QDs and metallic NPs. Unfortunately, little attention has been paid to the emission intensity of the semiconductor QDs and absorption efficiency of the metallic NPs, although both of these two factors also determine the rate of energy transfer. From an extensive literature survey, just simple QDs such as CdS,[13,14] CdSe,[15,18] and CdTe[19] have been used as energy donors. However, the photoluminescence (PL) emission spectra of these simple QDs could only be adjusted by changing the particle size through the reaction time. As the PL emission intensity of these QDs was also affected by the reaction time, it was very difficult to synthesize simple QDs not only with optimal emission spectra, but also with the best emission intensity. On the other hand, Au NPs as the most popular energy acceptors were often anchored on bioprobes, and one bioprobe was only labelled with one single Au NP. Yet, as the quantity of the bioprobes immobilized on the electrode was very limited, the SPR absorption efficiency of all of the anchored Au NPs was insufficient,

[a] *State Key Laboratory of Analytical Chemistry for Life Science, School of Chemistry & Chemical Engineering, Nanjing University, Nanjing, 210093, P. R. China. E-mail: jrzhang@nju.edu.cn, jjzhu@nju.edu.cn; Fax: +86 25 83686130; Tel: +86 25 83686130*

[b] *Institute of Advanced Materials, Nanjing University of Posts and Telecommunications, Nanjing 210046, P. R. China*

[c] *School of Chemistry and Life Science, Nanjing University Jinling college, Nanjing 210089, P. R. China*

† Electronic supplementary information (ESI) available: Experimental details; HRTEM images of the CdSeTe AQDs and Au NPs; EDX spectrum of the TiO_2:NNTs electrode; optimization of the Te/Se ratio in CdSeTe AQDs; optimization of the coating number of CdSeTe AQDs; concentration optimization of NH_2–DNA and thrombin aptamer; Comparison of using SiO_2@Au NCs and Au NPs as energy acceptors; selectivity, reproducibility and stability of the aptasensor. See DOI: 10.1039/c5cc01935d

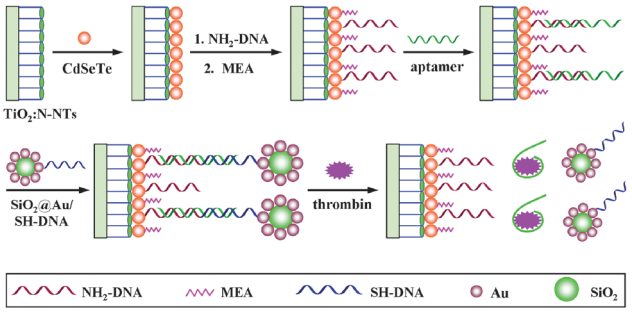

Scheme 1 Fabrication process of the photoelectrochemical aptasensor.

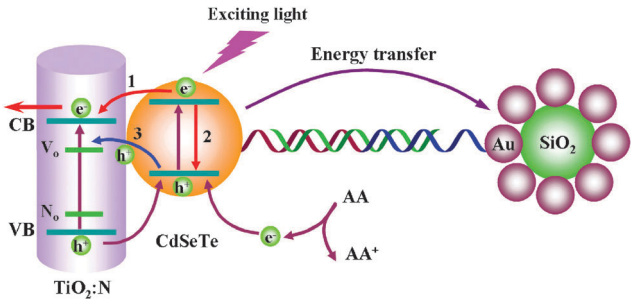

Scheme 2 Photoelectrochemical mechanism of the aptasensor.

leading to inefficient exciton energy transfer of the photoelectrochemical system.

Herein, we used CdSeTe alloyed quantum dots (AQDs) as energy donors and SiO_2@Au nanocomposites (NCs) as energy acceptors to construct an enhanced photoelectrochemical aptasensing platform, as shown in Scheme 1. As energy donors, CdSeTe AQDs offered great tunability of the PL emission band through adjusting the Te/Se ratio rather than changing the particle size. Thus, high quality luminescent QDs with optimal emission spectra could easily be obtained. Besides, according to quantum-mechanical calculations, the alloyed structure could also decrease the surface-related nonradiative decay, which in turn further promoted the PL emission intensity.[20] As energy acceptors, SiO_2@Au NCs could furnish plenty of Au NPs anchored on the DNA probes, which significantly enhanced the SPR absorption efficiency. Experimentally, we used thrombin as the target analyte to illustrate the proposed aptasensing platform. Firstly, CdSeTe AQDs were assembled on the surface of a nitrogen doped TiO_2 nanotube (TiO_2:N-NT) electrode by electrostatic adsorption. Then, NH_2–DNA was immobilized on the TiO_2:N-NT/CdSeTe electrode *via* the classic EDC coupling reaction between carbonyl groups on the surface of the CdSeTe AQDs and amino groups of the NH_2–DNA. After monoethanolamine (MEA) blocked unbound sites of the electrode surface, the thrombin aptamer and SiO_2@Au/SH-DNA were introduced, allowing NH_2–DNA as well as SH–DNA to hybridize with the thrombin aptamer. In this case, both the excitons of the CdSeTe AQDs and the SPR of the SiO_2@Au NCs could be induced simultaneously, leading to fast and efficient generation of energy transfer. However, in the presence of thrombin, the thrombin aptamer specifically bound with thrombin, and meanwhile SiO_2@Au/SH–DNA was released from the electrode surface, resulting in no energy transfer.

The photoelectrochemical mechanism of the proposed aptasensor is shown in Scheme 2. N-doping has introduced two electronic states into the TiO_2-NTs: N-doping at oxygen sites (N_O)[21] and oxygen vacancies (V_O).[22] Upon light irradiation, the photoexcited TiO_2:N-NTs and CdSeTe AQDs generated electron–hole pairs (excitons). And the electrons located at the conduction band (CB), whereas the holes located at the valence band (VB). The photogenerated electrons in CdSeTe AQDs had two major flow directions. One was electron transfer (process 1), which increased the photocurrent intensity of the aptasensor. The other was electron–hole recombination (process 2), which decreased the photocurrent intensity of the aptasensor. The two processes compete against each other. As the photoluminescence produced by electron–hole recombination of CdSeTe AQDs could generate SPR absorption of the Au NPs, energy transfer occurred. Meanwhile, a local electric field formed around the Au NPs, which in turn enhanced the electron–hole recombination rate of the CdSeTe AQDs.[23,24] Thus, energy transfer could be utilized to control the electron transfer process. Before the aptasensor was incubated with thrombin, high-efficient exciton energy transfer between the CdSeTe AQDs and SiO_2@Au NCs occurred. In this case, the electron–hole recombination process was dominant, whereas the electron transfer process was greatly suppressed, leading to low photocurrent intensity. After the aptasensor was incubated with thrombin, the exciton energy transfer was destroyed, and the electron transfer process was activated. At this time, as the TiO_2:N-NTs not only loaded plenty of CdSeTe AQDs but also effectively inhibited electron–hole recombination, the photocurrent intensity dramatically increased. Accordingly, the target analyte thrombin could be sensitively detected. The specific details are presented below.

To confirm successful synthesis of the CdSeTe AQDs and Au NPs, high resolution transmission electron microscopy (HRTEM) was performed (Fig. S1, ESI†). For efficient exciton energy transfer, spectral overlap between the emission spectra of the CdSeTe AQDs and absorption spectra of the Au NPs is essential. It can be seen from Fig. 1A that the CdSeTe AQDs show a strong PL emission peak at 517 nm (curve a), whereas the Au NPs exhibit a dominant plasmon absorption peak at about 515 nm (curve b). Notably, the PL emission of the CdSeTe AQDs has a considerable spectral overlap with the SPR absorption of the Au NPs, which was very favorable for inducing the SPR of the Au NPs. In addition, the distance between the CdSeTe AQDs and Au NPs on the sensing electrode was equal to the total length of NH_2–DNA and SH–DNA, namely 26 bases or about 9 nm. Thus, interparticle energy transfer between the CdSeTe AQDs and Au NPs would surely happen.

Fig. 1B displays the UV-vis spectrum of the formed SiO_2@Au/SH–DNA. As shown in curve a, the SH–DNA solution exhibited a sharp absorption peak located at 260 nm, which corresponds to the characteristic peak of DNA, generated from the absorption of purine and thymine bases. It can be seen from curve b that the pure SiO_2 NP aqueous suspension did not exhibit any evident absorption peak in the wavelength range. After the Au NPs were coated on SiO_2 NPs, an obvious plasmon absorption peak at

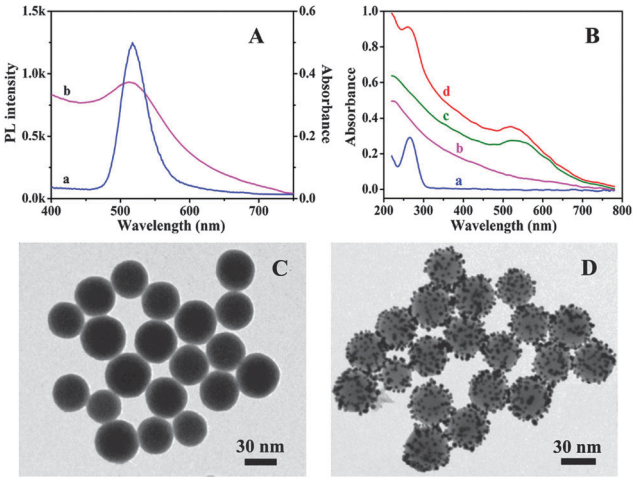

Fig. 1 (A) PL emission spectrum of (a) CdSeTe AQDs and (b) absorption spectrum of Au NPs; (B) UV-vis absorption spectra of (a) SH–DNA, (b) SiO_2 NPs, (c) SiO_2@Au NCs, and (d) SiO_2@Au/SH–DNA; TEM images of (C) SiO_2 NPs and (D) SiO_2@Au NCs.

525 nm appeared in curve c and a moderate red-shift (10 nm) could be found compared with the bare Au NPs (515 nm), indicating the formation of SiO_2@Au NCs.[25] While SH–DNA was covalently bound on the SiO_2@Au NCs, the characteristic peak of DNA located at 260 nm appeared in curve d and the plasmon absorption peak blue-shifted to 520 nm.[26] Thus, the UV-vis spectra suggested successful fabrication of SiO_2@Au/SH–DNA. Moreover, transmission electron microscopy (TEM) was also performed to characterize the SiO_2 NPs and SiO_2@Au NCs, as shown in Fig. 1C and D. Clearly, the pure SiO_2 NPs exhibited uniform size distribution and smooth surfaces with an average diameter of about 35 nm. After the SiO_2 NPs bound with Au NPs, many small-sized Au NPs scattered on the surface of the SiO_2 NPs, indicating successful formation of the SiO_2@Au NCs.

A highly ordered TiO_2-NT electrode is an excellent substrate material for constructing various photoelectrochemical biosensors because of its high stability, photoelectric activity, low cost, and biocompatibility.[27] Moreover, it possesses a large surface area, which can load large quantities of CdSeTe AQDs to evidently enhance the photocurrent intensity. In order to further enhance the photocurrent response, elemental N was doped into TiO_2-NTs, because the doped N created electronic states in the midgap region of TiO_2, which could facilitate hole-transfer from CdSeTe to TiO_2 (process 3, Scheme 2), leading to reduced electron–hole recombination of the CdSeTe AQDs.[28] Thus, a TiO_2:N-NT electrode was employed as the substrate to construct the photoelectrochemical aptasensor. Fig. 2A presents the typical SEM image of the TiO_2:N-NT electrode, which reveals that highly ordered nanotubes with an average inner diameter of about 18 nm have been well fabricated on the titanium sheet. Fig. S2 (see ESI†) shows the EDX spectrum of the TiO_2:N-NT electrode, and it confirms the presence of N in the TiO_2:NTs. As shown in Fig. 2B, the photocurrent response of the TiO_2:N-NT electrode was more or less the same as the TiO_2-NT electrode, because the formed V_O levels are located well below the hydrogen reduction potential (H_2O/H_2);[26] whereas the photocurrent response of the TiO_2:N-NT/CdSeTe electrode was nearly double that of the TiO_2-NT/CdSeTe electrode.

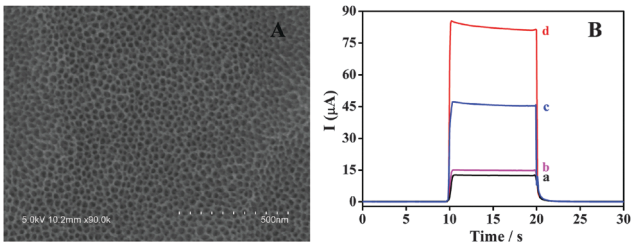

Fig. 2 (A) Typical SEM image of the TiO_2:N-NT electrode; (B) photocurrent intensity of (a) TiO_2-NT, (b) TiO_2:N-NT, (c) TiO_2-NT/CdSeTe, and (d) TiO_2:N-NT/CdSeTe electrodes.

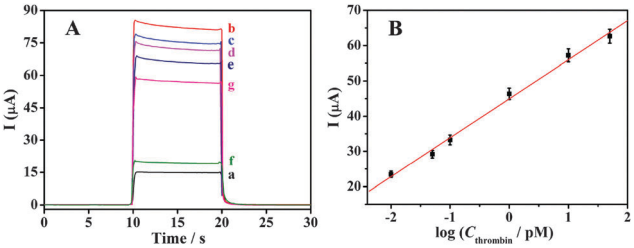

Fig. 3 (A) Photocurrent responses of (a) the TiO_2:N-NT electrode, (b) after CdSeTe AQD assembly, (c) after NH_2–DNA immobilization, (d) after MEA blocking, (e) after thrombin aptamer immobilization, (f) after SiO_2@Au/SH–DNA immobilization, and (g) after incubation with 20 μL of 10 pM thrombin; (B) calibration curve of the aptasensor for the detection of different concentrations of thrombin from 10 fM to 50 pM. The error bars show the standard deviation of five replicate determinations.

Hence, the photocurrent characterization proved that N-doping effectively inhibited electron–hole recombination of the CdSeTe AQDs. As the thickness of the CdSeTe film could influence the photocurrent intensity of the TiO_2:N-NT/CdSeTe electrode, the coating number of the CdSeTe AQDs was optimized (see Section 5 in ESI†). Thus, four coating numbers of CdSeTe AQDs were selected to fabricate the sensing electrode.

The construction process of the aptasensor could be monitored by photocurrent response, as shown in Fig. 3A. The TiO_2:N-NT electrode exhibited a relatively low photocurrent response (curve a) because of its limited absorption of ultraviolet light. After CdSeTe AQD immobilization, the photocurrent intensity (curve b) increased to about six times higher than that of the TiO_2:N-NT electrode, because the TiO_2:N-NT electrode loaded large quantities of the CdSeTe AQDs, and the modified CdSeTe AQDs increased absorbance of the exciting light, and meanwhile the doped N inhibited electron–hole recombination of the CdSeTe AQDs. Subsequently, the photocurrent intensity decreased after NH_2–DNA, MEA and the thrombin aptamer were successively immobilized on the CdSeTe AQD modified electrode (curves c–e), which could be attributed to the relatively weak charge transfer of DNA sequences as well as small organic molecules. After SiO_2@Au/SH–DNA immobilization, the photocurrent dramatically decreased (curve f), which was ascribed to exciton energy transfer from the CdSeTe AQDs to SiO_2@Au NCs. To illustrate the high SPR absorption efficiency of the SiO_2@Au NCs, bare Au NPs were used as energy acceptors for comparison. After Au/SH–DNA incubation, the photocurrent decreased moderately, which was only about 39% of that after

SiO_2@Au/SH–DNA immobilization, demonstrating the superiority of the SiO_2@Au NCs as energy acceptors (see Section 7 in ESI†). When the as-prepared sensing electrode was incubated with 20 μL of 10 pM thrombin, the photocurrent intensity significantly recovered (curve g). This was because the thrombin aptamer had specifically bound with thrombin, and meanwhile SiO_2@Au/SH–DNA was released from the electrode surface, leading to destroyed exciton energy transfer. Thus, the photocurrent responses proved the successful construction of the proposed aptasensor.

After confirming efficient exciton energy transfer between the CdSeTe AQDs and SiO_2@Au NCs and the successful construction of the aptasensor, the system was used for the photoelectrochemical detection of thrombin as a model. As shown in Fig. 3B, the photocurrent response linearly increased with an increase of the logarithm of thrombin concentration in the range of 10 fM to 50 pM. The regression equation is $I = 44.93 + 11.06 \log C$ (pM), with a correlation coefficient of 0.9967. The detection limit (S/N = 3) for thrombin concentration was estimated to be 2.8 fM, which is about 1–3 order(s) of magnitude better than recently reported, highly sensitive biosensors for thrombin detection.[29–34] The selectivity, reproducibility and stability of the aptasensor were also evaluated (see Section 8 in ESI†) and the results showed satisfactory specificity, acceptable reproducibility, and good stability of the aptasensor.

In summary, we constructed an enhanced photoelectrochemical aptasensing platform based on energy transfer between CdSeTe AQDs and SiO_2@Au NCs. As energy donors, the CdSeTe AQDs have less surface defects and high emission intensity, which obviously increased the exciton numbers. As energy acceptors, SiO_2@Au NCs could offer plenty of Au NPs, which evidently enhanced the absorption efficiency of exciton energy. The synergistic effect of the CdSeTe AQDs and SiO_2@Au NCs contributed to high-efficient exciton energy transfer. On the basis of the proposed aptasensing platform, thrombin was used as a detection model, and the aptasensor exhibited good analytical performances such as ultralow detection limit, wide linear response range, good selectivity, reproducibility, and stability. As different aptamers could specifically recognize different biomolecules, the well-established photoelectrochemical aptasensing platform has a universal and promising application in various bioanalyses.

We gratefully appreciate the support from the National Basic Research Program (2011CB933502) and the National Natural Science Foundation (21375059, 21175065, and 21335004) of China.

Notes and references

1 N. Haddour, J. Chauvin, C. Gondran and S. Cosnier, *J. Am. Chem. Soc.*, 2006, **128**, 9693–9698.
2 M. M. Liang, S. L. Liu, M. Y. Wei and L. H. Guo, *Anal. Chem.*, 2006, **78**, 621–623.
3 X. R. Zhang, Y. S. Guo, M. S. Liu and S. S. Zhang, *RSC Adv.*, 2013, **3**, 2846–2857.
4 G. L. Wang, P. P. Yu, J. J. Xu and H. Y. Chen, *J. Phys. Chem. C*, 2009, **113**, 11142–11148.
5 G. L. Wang, J. J. Xu, H. Y. Chen and S. Z. Fu, *Biosens. Bioelectron.*, 2009, **25**, 791–796.
6 X. Zhao, S. Zhou, L. P. Jiang, W. Hou, Q. Shen and J. J. Zhu, *Chem. – Eur. J.*, 2012, **18**, 4974–4981.
7 Y. An, L. Tang, X. Jiang, H. Chen, M. Yang, L. Jin, S. Zhang, C. Wang and W. Zhang, *Chem. – Eur. J.*, 2010, **16**, 14439–14446.
8 W. W. Zhao, Z. Y. Ma, P. P. Yu, X. Y. Dong, J. J. Xu and H. Y. Chen, *Anal. Chem.*, 2012, **84**, 917–923.
9 W. W. Zhao, Z. Y. Ma, D. Y. Yan, J. J. Xu and H. Y. Chen, *Anal. Chem.*, 2012, **84**, 10518–10521.
10 Y. J. Li, M. J. Ma and J. J. Zhu, *Anal. Chem.*, 2012, **84**, 10492–10499.
11 G. C. Fan, X. L. Ren, C. Zhu, J. R. Zhang and J. J. Zhu, *Biosens. Bioelectron.*, 2014, **59**, 45–53.
12 G. C. Fan, L. Han, J. R. Zhang and J. J. Zhu, *Anal. Chem.*, 2014, **86**, 10877–10884.
13 W. W. Zhao, J. Wang, J. J. Xu and H. Y. Chen, *Chem. Commun.*, 2011, **47**, 10990–10992.
14 W. W. Zhao, P. P. Yu, Y. Shan, J. Wang, J. J. Xu and H. Y. Chen, *Anal. Chem.*, 2012, **84**, 5892–5897.
15 X. Zhang, Y. Xu, Y. Yang, X. Jin, S. Ye, S. S. Zhang and L. Jiang, *Chem. – Eur. J.*, 2012, **18**, 16411–16418.
16 K. E. Sapsford, L. Berti and I. L. Medintz, *Angew. Chem., Int. Ed.*, 2006, **45**, 4562–4588.
17 N. C. Tansil and Z. Q. Gao, *Nano Today*, 2006, **1**, 28–37.
18 Q. Shen, L. Han, G. Fan, E. S. Abdel-Halim, L. Jiang and J. J. Zhu, *Biosens. Bioelectron.*, 2015, **64**, 449–455.
19 X. Zeng, S. Ma, J. Bao, W. Tu and Z. Dai, *Anal. Chem.*, 2013, **85**, 11720–11724.
20 D. D. Sarma, A. Nag, P. K. Santra, A. Kumar, S. Sapra and P. Mahadevan, *J. Phys. Chem. Lett.*, 2010, **1**, 2149–2153.
21 C. D. Valentin, G. Pacchioni, A. Selloni, S. Livraghi and E. Giamello, *J. Phys. Chem. B*, 2005, **109**, 11414–11419.
22 S. Livraghi, M. C. Paganini, E. Giamello, A. Selloni, C. D. Valentin and G. Pacchioni, *J. Am. Chem. Soc.*, 2006, **128**, 15666–15671.
23 A. O. Govorov, G. W. Bryant, W. Zhang, T. Skeini, J. Lee, N. A. Kotov, J. M. Slocik and R. R. Naik, *Nano Lett.*, 2006, **6**, 984–994.
24 J. Lee, P. Hernandez, J. Lee, A. O. Govorov and N. A. Kotov, *Nat. Mater.*, 2007, **6**, 291–295.
25 J. Xue, C. Wang and Z. Ma, *Mater. Chem. Phys.*, 2007, **105**, 419–425.
26 J. J. Storhoff, R. Elghanian, R. C. Mucic, C. A. Mirkin and R. L. Letsinger, *J. Am. Chem. Soc.*, 1998, **120**, 1959–1964.
27 Q. Kang, L. Yang, Y. Chen, S. Luo, L. Wen, Q. Cai and S. Yao, *Anal. Chem.*, 2010, **82**, 9749–9754.
28 J. Hensel, G. M. Wang, Y. Li and J. Z. Zhang, *Nano Lett.*, 2010, **10**, 478–483.
29 Z. Lin, L. Chen, X. Zhu, B. Qiu and G. Chen, *Chem. Commun.*, 2010, **46**, 5563–5565.
30 X. Li, L. Sun, A. Ge and Y. Guo, *Chem. Commun.*, 2011, **47**, 947–949.
31 X. Zhang, S. Li, X. Jin and S. S. Zhang, *Chem. Commun.*, 2011, **47**, 4929–4931.
32 Y. Chen, B. Jiang, Y. Xiang, Y. Chai and R. Yuan, *Chem. Commun.*, 2011, **47**, 7758–7760.
33 J. Zhang, Y. Chai, R. Yuan, Y. Yuan, L. Bai, S. Xie and L. Jiang, *Analyst*, 2013, **138**, 4558–4564.
34 Y. Wu, W. Xu, L. Bai, Y. Yuan, H. Yi, Y. Chai and R. Yuan, *Biosens. Bioelectron.*, 2013, **50**, 50–56.

